NAVAL POSTGRADUATE SCHOOL
Monterey, California

THESIS

ESTIMATION OF RANGE ERROR IN BISTATIC SONAR

by

John Charles Nygaard

March 1991

Thesis Advisor: Alan B. Coppens

UNCLASSIFIED

SECURITY CLASSIFICATION OF THIS PAGE

REPORT DOCUMENTATION PAGE

Form Approved OMB No. 0704-0188

1a REPORT SECURITY CLASSIFICATION: UNCLASSIFIED	1b. RESTRICTIVE MARKINGS
2a. SECURITY CLASSIFICATION AUTHORITY	3. DISTRIBUTION/AVAILABILITY OF REPORT: Approved for public release; distribution is unlimited
2b. DECLASSIFICATION/DOWNGRADING SCHEDULE	
4. PERFORMING ORGANIZATION REPORT NUMBER(S)	5. MONITORING ORGANIZATION REPORT NUMBER(S)
6a. NAME OF PERFORMING ORGANIZATION: Naval Postgraduate School; 6b. OFFICE SYMBOL (If applicable): PH	7a. NAME OF MONITORING ORGANIZATION: Naval Postgraduate School
6c. ADDRESS (City, State, and ZIP Code): Monterey, CA 93943-5000	7b. ADDRESS (City, State, and ZIP Code): Monterey, CA 93943-5000
8a. NAME OF FUNDING/SPONSORING ORGANIZATION; 8b. OFFICE SYMBOL (If applicable)	9. PROCUREMENT INSTRUMENT IDENTIFICATION NUMBER
8c. ADDRESS (City, State, and ZIP Code)	10. SOURCE OF FUNDING NUMBERS: PROGRAM ELEMENT NO. / PROJECT NO. / TASK NO. / WORK UNIT ACCESSION NO.

11. TITLE (Include Security Classification)
ESTIMATION OF RANGE ERROR IN BISTATIC SONAR

12. PERSONAL AUTHOR(S)
NYGAARD, John C.

13a. TYPE OF REPORT	13b. TIME COVERED	14. DATE OF REPORT (Year, Month, Day)	15. PAGE COUNT
Master's Thesis	FROM _____ TO _____	1991 March	57

16. SUPPLEMENTARY NOTATION The views expressed in this thesis are those of the author and do not reflect the official policy or position of the Department of Defense or the US Government.

17. COSATI CODES			18. SUBJECT TERMS (Continue on reverse if necessary and identify by block number)
FIELD	GROUP	SUB-GROUP	bistatic sonar; low frequency active sonar; active sonar; bistatic ellipse

19. ABSTRACT (Continue on reverse if necessary and identify by block number)

This thesis examines the range error propagation and uncertainties associated with bistatic sonar operations. An equation for determining range to the target from the receiver is explored for feasibility of practical applications. This particular equation does not require the separation distance between the source and receiver however, it does require an assumption of the mean sound speed over the two paths of the signal even though it could change drastically over a few miles. This thesis explores the contribution of eccentricity on the bistatic ellipse and the associated error. Examples demonstrate these effects by comparing cases of unequal mean sound speeds over the different paths at different values of eccentricity.

20. DISTRIBUTION/AVAILABILITY OF ABSTRACT	21. ABSTRACT SECURITY CLASSIFICATION
☑ UNCLASSIFIED/UNLIMITED ☐ SAME AS RPT. ☐ DTIC USERS	UNCLASSIFIED
22a. NAME OF RESPONSIBLE INDIVIDUAL: COPPENS, A.B.	22b. TELEPHONE (Include Area Code): 408-646-2941; 22c. OFFICE SYMBOL: PH/Cz

DD Form 1473, JUN 86 — Previous editions are obsolete. — SECURITY CLASSIFICATION OF THIS PAGE

S/N 0102-LF-014-6603 — UNCLASSIFIED

Approved for public release; distribution is unlimited

Estimation of Range Error in Bistatic Sonar

by

John Charles Nygaard
Lieutenant, United States Navy
B.S., Auburn University, 1984

Submitted in partial fulfillment of the
requirements for the degree of

MASTER OF SCIENCE IN APPLIED SCIENCE

from the

NAVAL POSTGRADUATE SCHOOL
March 1991

Author: _____
John Charles Nygaard

Approved by: _____
Alan B. Coppens, Thesis Advisor

_____
Harvey A. Dahl, Co-Advisor

_____
James N. Eagle, Chairman
Antisubmarine Warfare Academic Group

ABSTRACT

This thesis examines the range error propagation and uncertainties associated with bistatic sonar operations. An equation for determining range to the target from the receiver is explored for feasibility of practical applications. This particular equation does not require the separation distance between the source and receiver however, it does require an assumption of the mean sound speed over the two paths of the signal even though it could change drastically over a few miles. This thesis explores the contribution of eccentricity on the bistatic ellipse and the associated error. Examples demonstrate these effects by comparing cases of unequal mean sound speeds over the different paths at different values of eccentricity.

TABLE OF CONTENTS

I. INTRODUCTION

A. BACKGROUND

Early ASW relied solely on active sonar, or Echo Ranging. A pulse of sound was projected into the ocean and if a submarine was in the path of the signal, an echo would return. The round-trip time of travel of this signal was used with the sound speed in the ocean to determine the range to the target. This method of ASW was very effective until submarines began to exploit the water conditions of the ocean and became evasive, i.e., hiding in shadow zones, fronts and eddies, etc. The projected pulse from the active platform usually could be detected by the submarine at a substantially greater range than that at which the active platform could detect the reflected pulse from the target because of the greater transmission loss (TL) over the round trip propagation path [Ref. 1]. This was one of the factors leading to interest in passive sonar. Additionally, passive sonar often utilized lower frequencies having smaller losses, which could allow longer detection ranges [Ref. 2].

The structure of the speed-of-sound profile leads to a deep sound channel which can be exploited in convergence zone (CZ) propagation. This propagation mode with its intrinsically lower acoustic losses provides longer standoff ranges, keeping the detector out of torpedo ranges of the submarine. On the other hand, a disadvantage of passive sonar

is that it requires a relatively time-consuming process of bearing rate analysis known as Target Motion Analysis (TMA) to determine range to a target [Ref. 3]. Because of this, active sonar operations are still important, particularly for last minute, close-in prosecutions where exact range must be determined quickly for weapon deployment.

As technology advanced, passive sonar became more sensitive, permitting longer detection ranges. Submarines, however, reduced their radiated noise levels nullifying the advantages of the more sensitive sensors. This progressive technology also made way for the continued improvement of active sonar, extending capabilities to much lower frequencies, thus permitting active sonar exploitation of the deep sound channel. Bistatic Active Sonar (BAS) has brought about longer range detection by active sonar, and with it the advantage of immediate determination of the range to the target. Consequently, the vulnerability of active sonar platforms has been reduced with the technique of bistatic sonar operations.

B. BISTATIC SONAR

Conventional active sonar is monostatic, meaning that the source and receiver are usually on the same platform, as displayed in Figure 1. A pulse is generated by the source, transmitted to the target, reflected from the target, and the resultant echo transmitted back to the receiver. Directional

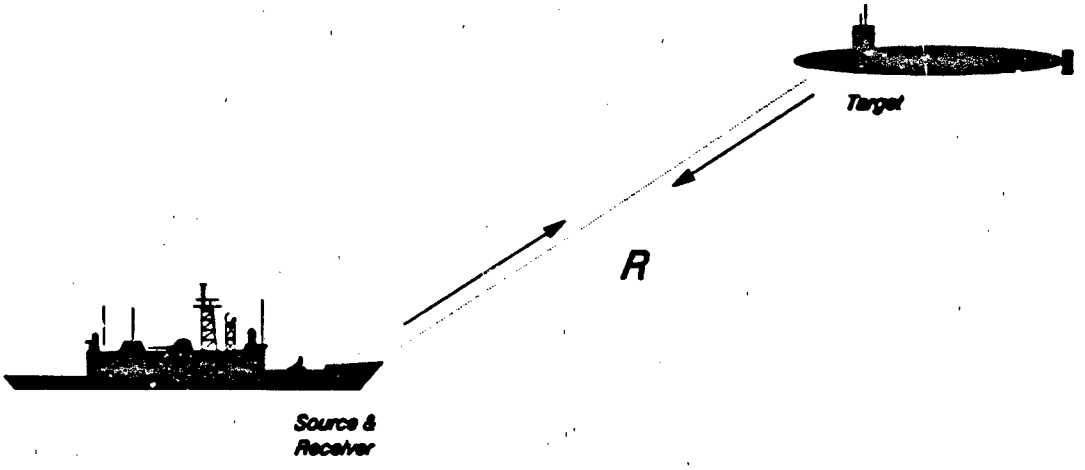

Figure 1 Monostatic Arrangement

sonar sensors provide an estimate of the bearing of the target and the range to the target is determined indirectly by the equation

$$Range = \frac{1}{2} t \cdot V \qquad (1.1)$$

where V is the sound speed in the ocean, and t is the round trip travel time of the pulse and echo.

Bistatic sonar has a separated source and receiver on two different platforms. Figure 2 is a representative bistatic arrangement [Ref. 4]. The receiver is positioned away from the source to receive the reflected signal from the target. In the bistatic case, the source, receiver, and target form a triangle which complicates the problem compared to the monostatic case because the range (R) is more difficult to determine. The source is presumably detached and away from the threat, reducing its own vulnerability. An active

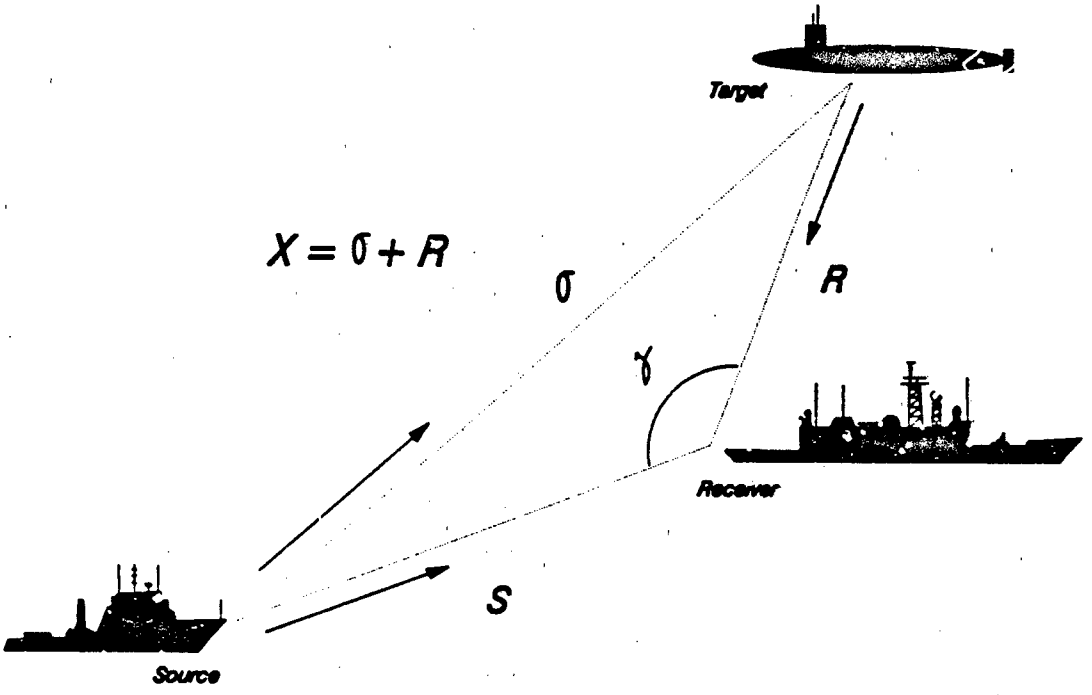

Figure 2 Bistatic Arrangement

signal, or "ping", originates at the source, travels to the target, is reflected from the target, and then travels to the receiver as shown by the arrows. The total travel distance of this signal is X. The receiver also receives a direct signal from the source over the path S. The angle (γ) is the separation angle of the source and the target measured at the receiver. The ultimate goal of such an operation is to obtain the bearing and range of a target with respect to the receiver. Since the bearing is directly obtainable from the directional sonar receiver, determining the range (R) is the problem that is to be treated here.

II. STATEMENT OF PROBLEM

A. RANGE EQUATION

An equation must be derived that solves for range (R) to the target in terms of known quantities. For our purposes, we shall assume that the total travel distances of the acoustic signal over the two paths between source and receiver, the distances X and S in Figure 2, are known. Then, given the bearing γ, we have

$$\sigma = X - R \tag{2.1}$$

and, from the law of cosines,

$$\sigma^2 = R^2 + S^2 - 2RS\cos\gamma. \tag{2.2}$$

Substitution of the first equation into the second allows the elimination of σ.

$$(X-R)^2 = R^2 + S^2 - 2RS\cos\gamma \tag{2.3}$$

Expanding the term on the left gives

$$X^2 - 2RX + R^2 = R^2 + S^2 - 2RS\cos\gamma. \tag{2.4}$$

Rearranging, we have

$$2RX - 2RS\cos\gamma = X^2 - S^2. \tag{2.5}$$

Solving for R results in [Ref. 5]

$$R = \frac{X^2 - S^2}{2(X - S\cos\gamma)}. \tag{2.6}$$

The above equation gives R in terms of S, X, and γ.

The time of travel of a signal from the source directly to the receiver over the path S is t_s, and the time of travel for the indirect route X is t_x. The difference between t_x and t_s is

$$t = t_x - t_s. \tag{2.7}$$

These time definitions, combined with the mean sound speed over the propagation path, determine the distance that the signal has traveled. Use of

$$X = Vt_x \text{ and } S = Vt_s \tag{2.8}$$

yields several different equations involving different combinations of the variables; V, S, X, t_x, t_s, t and γ [Ref. 6]. One such combination can be derived as follows. Substitution of (2.9) into (2.6), results in

$$R = \frac{(Vt_x)^2 - (Vt_s)^2}{2(Vt_x - Vt_s\cos\gamma)}, \tag{2.9}$$

and, the substitution of (2.7) for t_x provides

$$R = \frac{(V(t+t_s))^2 - (Vt_s)^2}{2(V(t+t_s) - Vt_s\cos\gamma)}. \tag{2.10}$$

Expanding both the numerator and the denominator leaves

$$R = \frac{V^2t^2 + 2V^2tt_s + V^2t_s^2 - V^2t_s^2}{2(Vt + Vt_s - Vt_s\cos\gamma)}, \tag{2.11}$$

and simplification gives

$$R = \frac{V^2 t^2 + 2V^2 t t_s}{2V(t + t_s - t_s \cos\gamma)}. \qquad (2.12)$$

Now, use of

$$1 - \cos\gamma = 2\sin^2\frac{\gamma}{2} \qquad (2.13)$$

produces

$$R = \frac{Vt(Vt + 2Vt_s)}{2V(t + t_s - t_s + 2t_s\sin^2(\frac{\gamma}{2}))} \qquad (2.14)$$

and therefore

$$R = \frac{t(Vt + 2Vt_s)}{2(t + 2t_s\sin^2\gamma/2)}. \qquad (2.15)$$

Now, use of the relationship

$$V = \frac{S}{t_s} \qquad (2.16)$$

gives

$$R = \frac{t\left(\frac{St}{t_s} + 2\frac{St_s}{t_s}\right)}{2(t + 2t_s\sin^2\gamma/2)} \qquad (2.17)$$

and finally

$$R = \frac{St(t + 2t_s)}{2t_s(t + 2t_s\sin^2\gamma/2)}. \qquad (2.18)$$

This equation, commonly encountered, is a function of S, t, t_s, and γ. Measured quantities of the variables used above are often known to much more precision than the value of the

mean sound speed V over many miles. Thus V has the largest amount of uncertainty, because the sound speed profile at the receiver must be assumed over the whole path of the signal. (Most bistatic sonar operations use a formula similar to Equation 2.18 to determine range from the receiver to the target [Ref. 6].) However, this thesis explores the use of an equation that contains V explicitly rather than S and also allows the treatment of different mean sound speeds. By using the variable S, there is an inherent assumption that S has a readily obtainable value. To see the advantages using V rather than S, it is appropriate to consider the role of ASW Command Control and Communications (C^3), few operational facts must be discussed.

B. C^3 CONSIDERATIONS

Since S is the distance between the source and receiver, an accurate position of the source must be known for the calculation of the separation distance, S. This requires that reliable communications be maintained between the two vessels carrying source or receiver (Figure 3). Ships that are within "line of sight" usually communicate by UHF (Ultra High Frequency) radio, which is extremely reliable, but very limited in range. When ships are separated by a distance greater than "line of sight", approximately 20 nm, other means of communication must be utilized. One such method is the HF (High Frequency) radio which has a longer range because of the radio wave propagation that follows the curvature of the earth

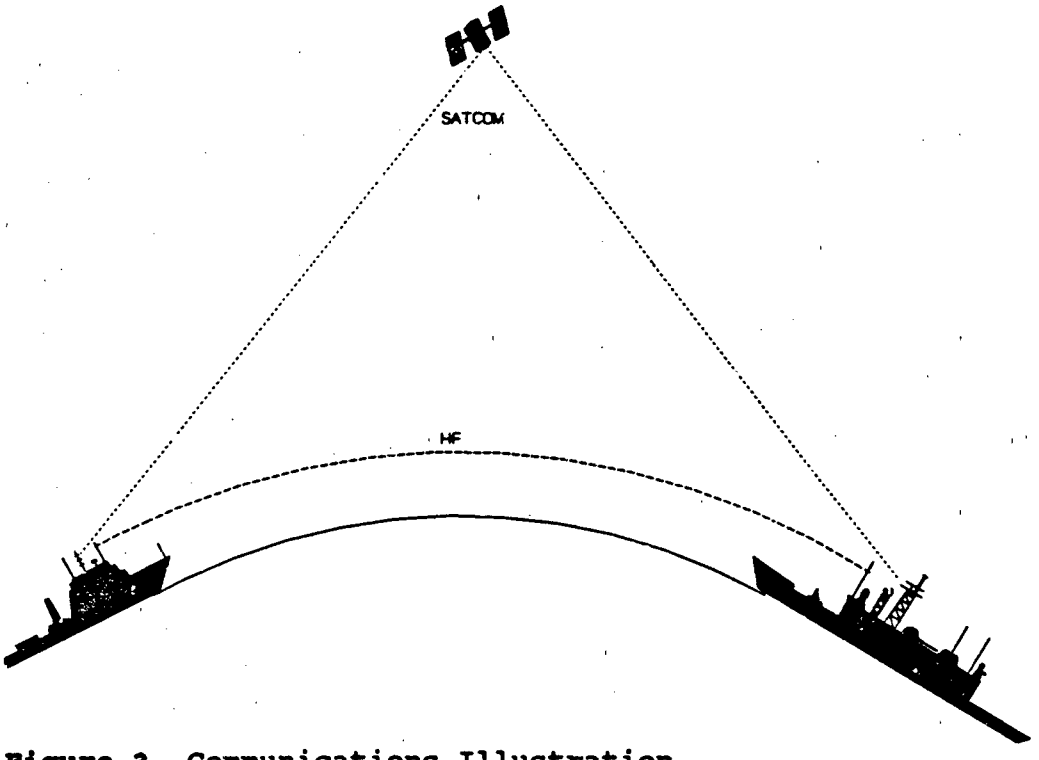

Figure 3 Communications Illustration

[Ref. 7]. The disadvantage of HF communications is that this type of communication is extremely dependent on atmospheric conditions, since atmospheric "ducting" is required. Another disadvantage of HF communications is the vulnerability of the HF transmitter to direction finding (DF) [Ref. 8] by an opponent. For example, there are Soviet HFDF sites around the world that can triangulate HF transmissions to determine the location of the transmitter. A third method of communicating over great distances is UHF Satellite communications (SATCOM). In this method, the UHF transmission is "bounced" off of a satellite to another station over the horizon. SATCOM is extremely reliable, and is indeed a preferred method, but in

the age of "killer satellites," dependency on satellites can be extremely limiting in operations.

If (2.18) were being used, then a communication link must be maintained. If this link is broken and communications are lost, there are two options to continue bistatic operations. The first option is that the source and receiver move to within line-of-sight UHF range, typically 20 nm. This would reduce the advantage of the bistatic concept because the receiver is not "out front" exploiting the submarines reflected energy, and decreasing the source's vulnerability. The second option in case of lost communications is for the receiver ship to approximate the source's position by applying the last known course and speed to the last known position, also known as Dead Reckoning (DR). This introduces significant error in the variable S.

An alternate means of locating the target using bistatic operations would be based on an equation that removes the necessity to know the distance S directly.

C. AN ALTERNATIVE EQUATION

To avoid the difficulties mentioned in the previous section, we return to (2.6),

$$R = \frac{X^2-S^2}{2(X-S\cos\gamma)}$$

and use the relationships

$$X = Ut_x \text{ and } S = Vt_s \qquad (2.19)$$

to introduce differences in the mean sound speed over the different paths, where U is the mean sound speed over the reflected path and V is the mean sound speed over the direct path. Substituting (2.19) into (2.6) results in

$$R = \frac{(Ut_x)^2 - (Vt_s)^2}{2(Ut_x - Vt_s Cos\gamma)}, \qquad (2.20)$$

and by dividing the numerator and denominator by V^2, it becomes

$$R = \frac{\left(\frac{U}{V}t_x\right)^2 - (t_s)^2}{\frac{2}{V}\left(\frac{U}{V}t_x - t_s \cos\gamma\right)}. \qquad (2.21)$$

A scaled time, τ_x, can be introduced to deal with these differences in speed, where

$$\tau_x = \frac{U}{V}t_x. \qquad (2.22)$$

Euqation (2.21) can now be rewritten as

$$R = \frac{V(\tau_x^2 - t_s^2)}{2(\tau_x - t_s \cos\gamma)}. \qquad (2.23)$$

The equation still requires values for τ_x, t_s, and γ, but S is no longer directly used. This thesis examines the utility of this equation (2.23) as an alternate to (2.18).

An important point to note is that in order for bistatic operations to take place, convergence zone conditions must exist, and for these to exist there must be a minimum of 200 fathoms of depth excess for reliable propagation [Ref. 3]. In

essence, bistatic operations usually must take place in the deep ocean and away from typical fronts and eddies where water conditions change drastically over short distances.

The feasibility of using this equation will be examined by means of error analysis. We include in this analysis the variation in mean sound speed between the two different paths as well as the uncertainties in bearing and in times of flight of signal and echo.

III. DEVELOPMENT OF ANALYSIS MODEL

Analysis of (2.23),

$$R = \frac{V(\tau_x^2 - t_s^2)}{2(\tau_x - t_s\cos\gamma)},$$

is conducted from the point of view that it is the equation of an ellipse. Indeed, any bistatic sonar geometry can be described in terms of ellipses, the properties of which relate directly to the sonar parameters.

A. INTRODUCTION OF ELLIPSE

Figure 4 is a diagram of a bistatic arrangement with a superimposed ellipse, where a is half the length of the major axis (the semi-major axis), and S is the distance between the two foci. The eccentricity (e) of an ellipse can be defined by the ratio e=S/2a. Use of the previously-defined relationships and properties of ellipses then provide additional expressions

$$e = \frac{S}{X} = \frac{S}{\sigma+R} = \frac{Vt_s}{Ut_x} = \frac{t_s}{\tau_x}. \qquad (3.1)$$

Equation (3.1) reveals that the effect of a difference between the mean sound speeds U and V over the two paths can be completely accounted for by making an adjustment in the eccentricity e of the ellipse. The manipulations that follow will result in convenient expressions for the fractional errors in range arising from uncertainties in timing errors,

differences between U and V, and bearing errors. The value of eccentricity may range between 0 and 1, where e = 0 is a perfect circle and e = 1 is a very flat ellipse approaching a straight line joining the foci. These elliptical relationships will be useful in describing the error associated with different geometries.

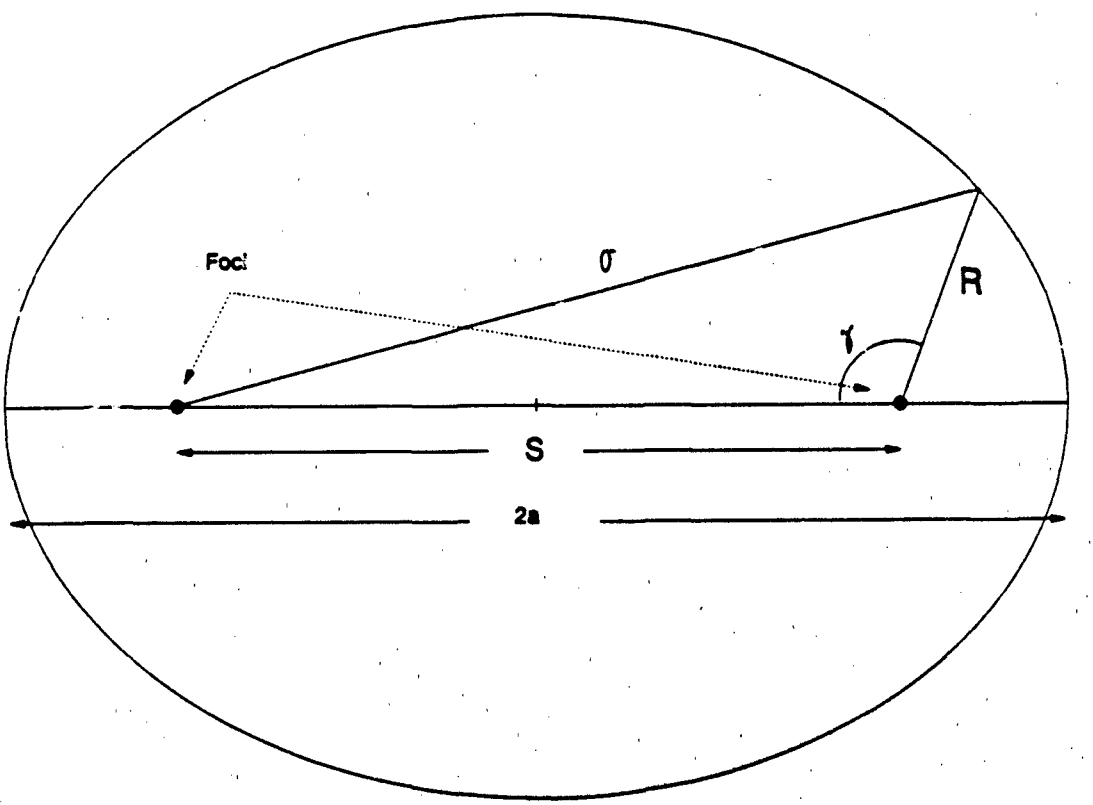

Figure 4 Elliptical Arrangement

B. DIFFERENTIATING TERMS

The error in range, ΔR, can be expressed in terms of the errors in V, τ_x, t_s, and γ as

$$\Delta R = \frac{\partial R}{\partial V}\Delta V + \frac{\partial R}{\partial \tau_x}\Delta \tau_x + \frac{\partial R}{\partial t_s}\Delta t_s + \frac{\partial R}{\partial \gamma}\Delta \gamma, \tag{3.2}$$

or, in the form of a fractional error, as

$$\frac{\Delta R}{R} = \frac{1}{R}\frac{\partial R}{\partial V}\Delta V + \frac{1}{R}\frac{\partial R}{\partial \tau_x}\Delta \tau_x + \frac{1}{R}\frac{\partial R}{\partial t_s}\Delta t_s + \frac{1}{R}\frac{\partial R}{\partial \gamma}\Delta \gamma. \tag{3.3}$$

The coefficients of the error increments ΔV, $\Delta \tau_x$, Δt_s, and $\Delta \gamma$ on the right side of the equation may be obtained by logarithmic partial differentiation of (2.23). The coefficient of ΔV in the first term on the right is

$$\frac{1}{R}\frac{\partial R}{\partial V} = \frac{1}{V}. \tag{3.4}$$

The coefficient in the second term is

$$\frac{1}{R}\frac{\partial R}{\partial \tau_x} = \frac{2\tau_x}{\tau_x^2 - t_s^2} - \frac{1}{\tau_x - t_s \cos\gamma}. \tag{3.5}$$

The coefficient in the third term is

$$\frac{1}{R}\frac{\partial R}{\partial t_s} = \frac{-2t_s}{\tau_x^2 - t_s^2} + \frac{\cos\gamma}{\tau_x - t_s \cos\gamma}. \tag{3.6}$$

Finally the coefficient in the γ term is

$$\frac{1}{R}\cdot\frac{\partial R}{\partial \gamma} = -\frac{t_s \sin\gamma}{\tau_x - t_s\cos\gamma} \tag{3.7}$$

If these coefficients are assembled, (3.3) may be rewritten as

$$\begin{aligned}\frac{\Delta R}{R} = \frac{\Delta V}{V} &+ \left(\frac{2\tau_x}{\tau_x^2 - t_s^2} - \frac{1}{\tau_x - t_s\cos\gamma}\right)\Delta\tau_x \\ &- \left(\frac{2t_s}{\tau_x^2 - t_s^2} - \frac{\cos\gamma}{\tau_x - t_s\cos\gamma}\right)\Delta t_s - \frac{t_s\sin\gamma}{\tau_x - t_s\cos\gamma}\Delta\gamma.\end{aligned} \tag{3.8}$$

Note: $\tau_x = \frac{U}{V}t_x$, $\Delta\tau_x = \frac{U}{V}\Delta t_x$, $\frac{\Delta\tau_x}{\tau_x} = \frac{\Delta t_x}{t_x}$, *and* $\frac{\Delta t_s}{\tau_x} = \frac{V}{U}\frac{\Delta t_s}{t_x}$

By incorporating the relationships described in (3.1) the above equation may be rewritten as

$$\begin{aligned}\frac{\Delta R}{R} = \frac{\Delta V}{V} &+ \left(\frac{2}{1-e^2} - \frac{1}{1-e\cos\gamma}\right)\frac{\Delta\tau_x}{\tau_x} \\ &+ \left(\frac{-2e}{1-e^2} + \frac{\cos\gamma}{1-e\cos\gamma}\right)\frac{\Delta t_x}{\tau_x} - \frac{e\sin\gamma}{1-e\cos\gamma}\Delta\gamma.\end{aligned} \tag{3.9}$$

C. MEAN SQUARE ERROR

The fractional error in range can be obtained through the use of this equation if all errors in the variables V, τ_x, t_s, and γ are known completely , both in magnitude and in direction. On the other hand, if all errors (i.e., uncertainties) in the variables V, τ_x, t_s, and γ are assumed to be statistically independent of each other, they may be

combined into a mean square error (MSE). The MSE is used to determine the total combined error resulting from errors in variables in the range equation. It is calculated by taking the square root of the sum of the squares of the individual errors. Each of the terms has an uncertainty value (Δ) associated with that particular variable, i.e., Δt_x. The correct numerical uncertainty values of each variable used operationally has a security classification and will not be used in this thesis. To simplify the notation in the model the coefficients of the error terms in (3.8) will be expressed as A_x, A_s or A_G, where

$$A_x = \left(\frac{2}{1-e^2} - \frac{1}{1-e\cos\gamma}\right),$$

$$A_s = \left(\frac{-2e}{1-e^2} + \frac{\cos\gamma}{1-e\cos\gamma}\right),$$

$$A_G = \frac{-e\sin\gamma}{1-e\cos\gamma}.$$

The use of these coefficients gives the fractional error in range in the form

$$\frac{\Delta R}{R} = \frac{\Delta V}{V} + A_x\frac{\Delta\tau_x}{\tau_x} + A_s\frac{\Delta t_s}{\tau_x} + A_G\Delta\gamma. \qquad (3.10)$$

The mean square fractional error is thus

$$\frac{1}{R}(\Delta R)_{rms} = \sqrt{\left(\frac{\Delta V}{V}\right)^2 + A_X^2\left(\frac{\Delta \tau_X}{\tau_X}\right)^2 + A_S^2\left(\frac{\Delta t_S}{\tau_X}\right)^2 + A_G^2(\Delta\gamma)^2}. \quad (3.11)$$

in which it is assumed that the errors on the right side of the equation are statistically independent. Equation 3.11 calculates error in terms of the fractional timing errors referenced to a time base of t_X. If it is preferable to express timing errors over each path referenced to the travel time over each path, then

$$\frac{\Delta R}{R} = \frac{\Delta V}{V} + A_X\frac{\Delta t_X}{t_X} + eA_S\frac{\Delta t_S}{t_S} + A_G\Delta\gamma. \quad (3.12)$$

Note: $e = \frac{Vt_S}{Ut_X}$, $\frac{1}{t_X} = \frac{U}{V}e\frac{1}{t_S}$

$$\frac{V}{U}A_S\frac{\Delta t_S}{t_X} = \frac{V}{U}A_S\frac{U}{V}e\frac{\Delta t_S}{t_S} = eA_S\frac{\Delta t_S}{t_S}$$

The mean square fractional error is then changed to

$$\frac{1}{R}(\Delta R)_{rms} = \sqrt{\left(\frac{\Delta V}{V}\right)^2 + A_X^2\left(\frac{\Delta t_X}{t_X}\right)^2 + e^2A_S^2\left(\frac{\Delta t_S}{t_S}\right)^2 + A_G^2(\Delta\gamma)^2} \quad (3.13)$$

To understand the use of these equations suppose we consider the general method by which the range from the receiver ship to the target (R) and the associated range error can be found. Assume, for example, that the signal travel times t_X and t_S, and the azimuth angle γ all have been measured. Assume, further, that the average sound speed V over the direct path from source to receiver is known. Also

let U, the average sound speed over the secondary path, source-to-target-to-receiver, be the same as V, so that $t_x = t_x$. The range R can then be calculated from 2.23, where

$$R = \frac{V(t_x^2 - t_s^2)}{2(t_x - t_s \cos\gamma)}.$$

Assume also that the uncertainties in time, Δt_x and Δt_s, and the uncertainties in azimuths, $\Delta\gamma$, are all known. The fractional error (uncertainty) in range associated with each of the uncertainties in the separate variables can be obtained as follows.

For timing error in t_x alone the corresponding fractional error in range is

$$\left(\frac{\Delta R}{R}\right)_x = A_x \frac{\Delta t_x}{t_x}. \qquad (3.14)$$

We obtain A_s from the graphs of Fig. 5 through 13 after first calculating the eccentricity,

$$e = \frac{S}{X} = \frac{t_s}{t_x},$$

for this particular case being studied. Similarly for error in t_s alone use

$$\left(\frac{\Delta R}{R}\right)_s = A_s \frac{\Delta t_s}{t_x} = e A_s \frac{\Delta t_s}{t_s}, \qquad (3.15)$$

and for error in γ use

$$\left(\frac{\Delta R}{R}\right)_G = A_G \Delta\gamma, \qquad (3.15)$$

where $\Delta\gamma$ must be in units of radians. If more than one of the independent variables is uncertain, then either (3.11) or (3.13) for the combined errors should be used.

D. ERROR ANALYSIS

A computer program was written to study the behavior in range error in each of the three variables t_x, t_s, and γ. The program, written in FORTRAN, was used for nine different values of eccentricity e of the basic range ellipse, from 0.1 to 0.9. The output data of the program, the values of A_x, A_s, and A_G, were plotted in the form of curves from which error estimates can be made for any reasonable scenarios.

IV. RESULTS AND VERIFICATION

A. RESULTS OF MODEL

Figures 5 through 13 are plots of the output data of the previously mentioned Fortran program. All of these plots indicate some relationships which will be examined further. Each of the nine figures is a graph of the error coefficients for a different eccentricity e, beginning with Figure 5 for the case of eccentricity 0.1 and continuing to Figure 13 with eccentricity of 0.9. In all of the plots the A_χ values are represented by solid lines, the A_S values are represented by dotted lines and the A_G values are indicated by dashed lines. The error coefficients (ordinates) give the magnitudes of the errors associated with each of the three terms. The baseline number (S) used for input is inconsequential because the value of e characterizes the driver in the error propagation. Each of the three terms will be evaluated individually.

The A_χ term is the indicator of the behavior of fractional error associated only with uncertainty in the value of t_χ. The graphs in the figures show how A_χ and the other error coefficients vary with bearing angle γ. The graphs reveal that for low values of eccentricity e, the error coefficient A_χ begins small and shows a small increase as γ increases to 180°. For large values of e, the values of A_χ remain small for low values of γ, but as γ increases, the A_χ value

increases rapidly until about mid range of γ, approximately 70°, when it levels off and approaches a maximum at 180°. This information indicates that for small values of e, the error contribution by the t_x term is small for all values of γ. On the other hand, for large values of eccentricity, the error contribution of t_x begins small for angles less than 10°, but rapidly increases for larger angles until it steadies out. In practical terms, recall that a small value of e means a small separation distance (S)between the source and receiver compared to the distance between the receiver and the target (R). Consequently, a smaller S means a smaller error associated with t_x. For larger values of e, the error contributed by t_x increases drastically for separation angles (γ) greater than 10°.

The A_s coefficient characterizes the effect of uncertainty in the time t_s. These values are represented by the dotted line on each of the nine graphs. For γ of 0° and 180° this error coefficient is about the same as for the previously determined A_x. For small values of e, A_s gradually decreases to zero, at about 70°, and then increases until it has the same value as A_x at 180°. For higher values of e, the value of A_s drops more rapidly to zero at angles less than 10° and then approaches the values of A_x as it increases sharply and behaves asymptotically done about 70°. The A_s coefficient goes to zero at moderate values of γ, about 70°, for low e, and it goes to zero at small angles for large e. When the

source and receiver are closer to each other than the receiver is to the target, this angle at which the error vanishes is around 70° to 80°, and for large values of e, this angle is much lower, near 10°.

The error coefficient A_G, associated with the γ term, is zero for γ values of 0° and 180°, as expected. For smaller values of e, the error coefficient increases slowly until it peaks at about 90°. For small values of e, the contribution of the γ remains small compared to the other two terms. For larger values of e, the maximum value of A_G increases significantly, and it "shifts" to smaller angles to the left as e increases. In practical terms, when the source is closer to the receiver than the target is to the receiver, that is, when S is less than R, the error contribution of the γ value is relatively insignificant. If the geometry is such that e is large, then the error would be reduced if the angle γ remains greater than 90°. All plots shown in the figures represent the absolute values of the error coefficients.

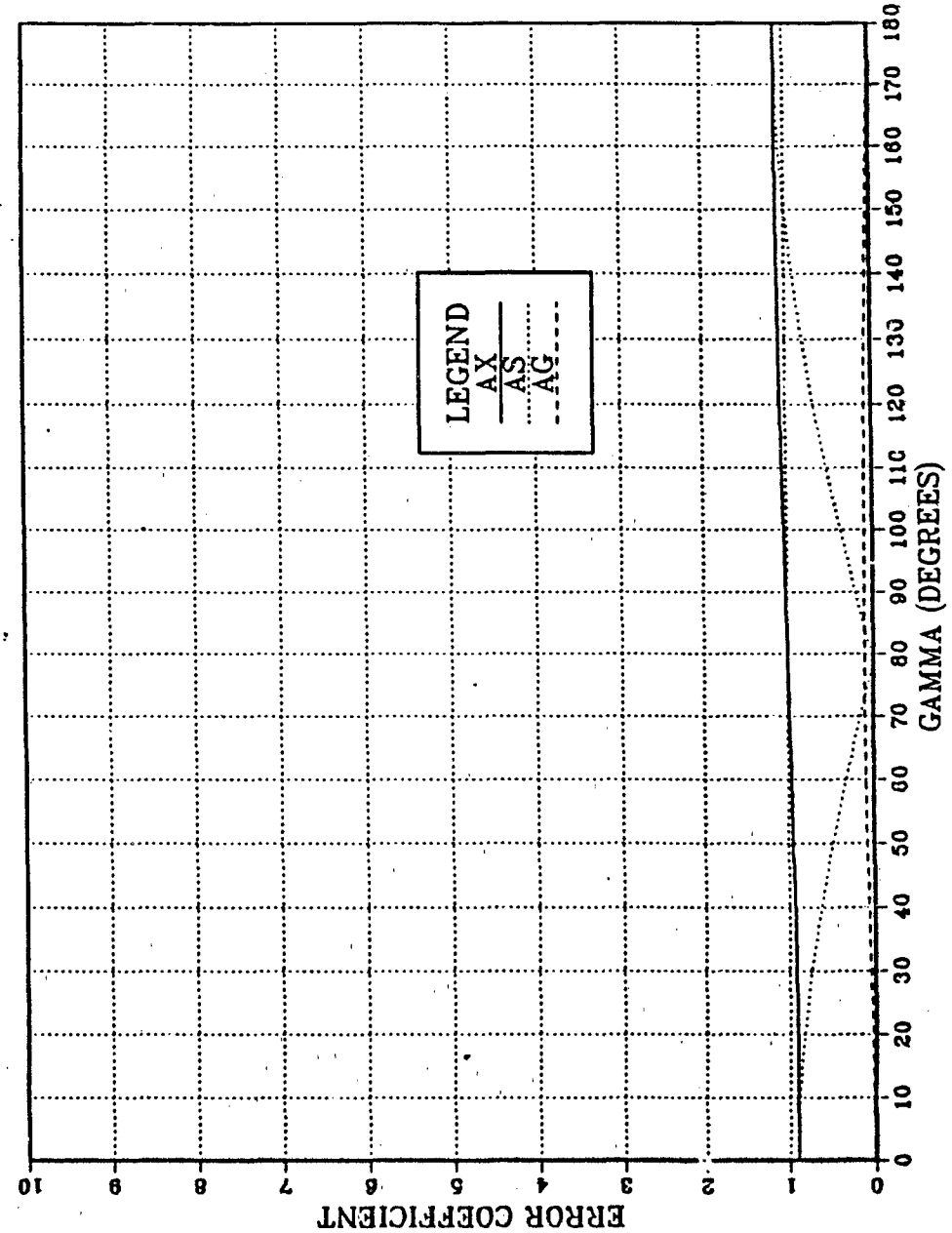

Figure 5 Error vs. Angle for e=0.1

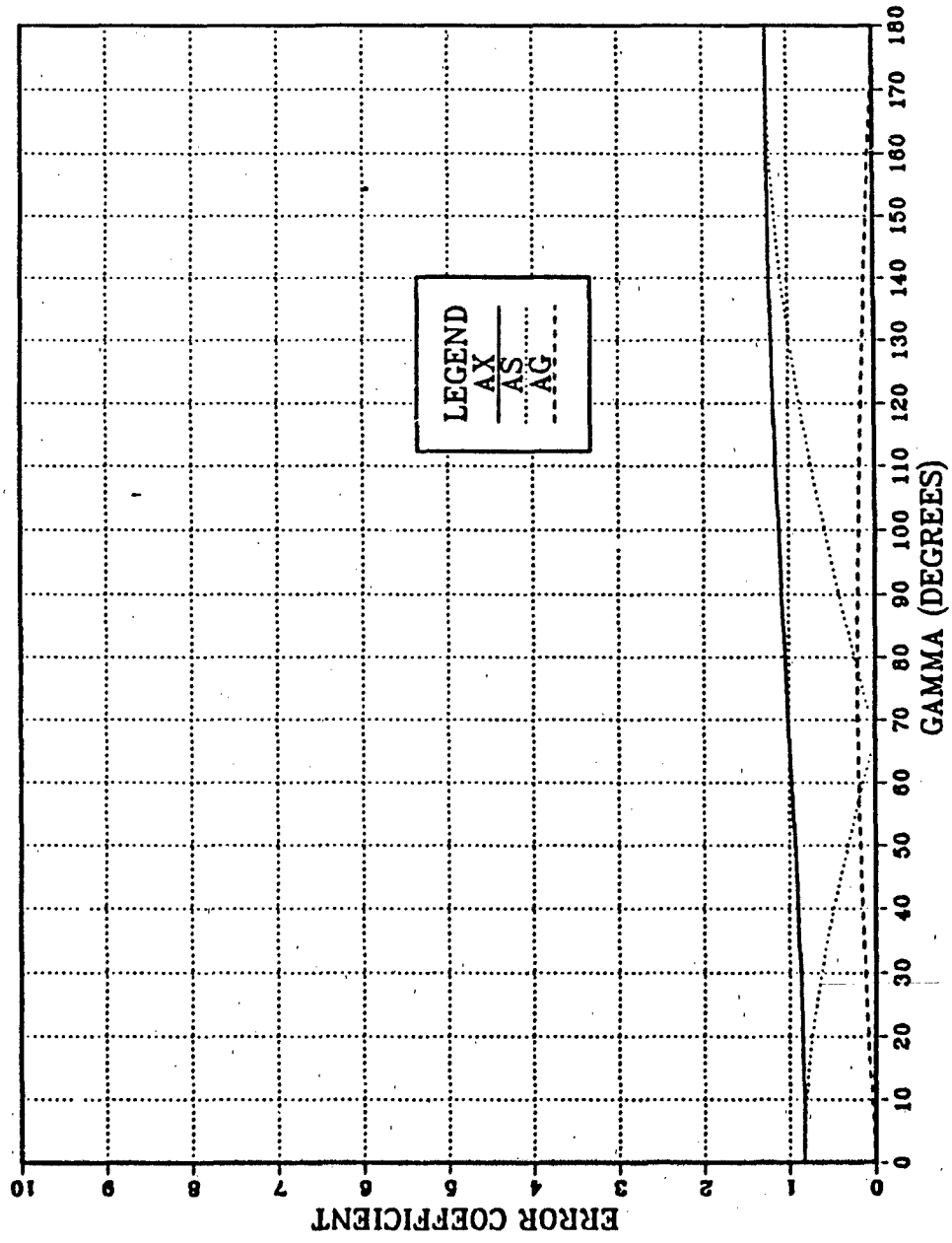

Figure 6 Error vs. Angle for e=0.2

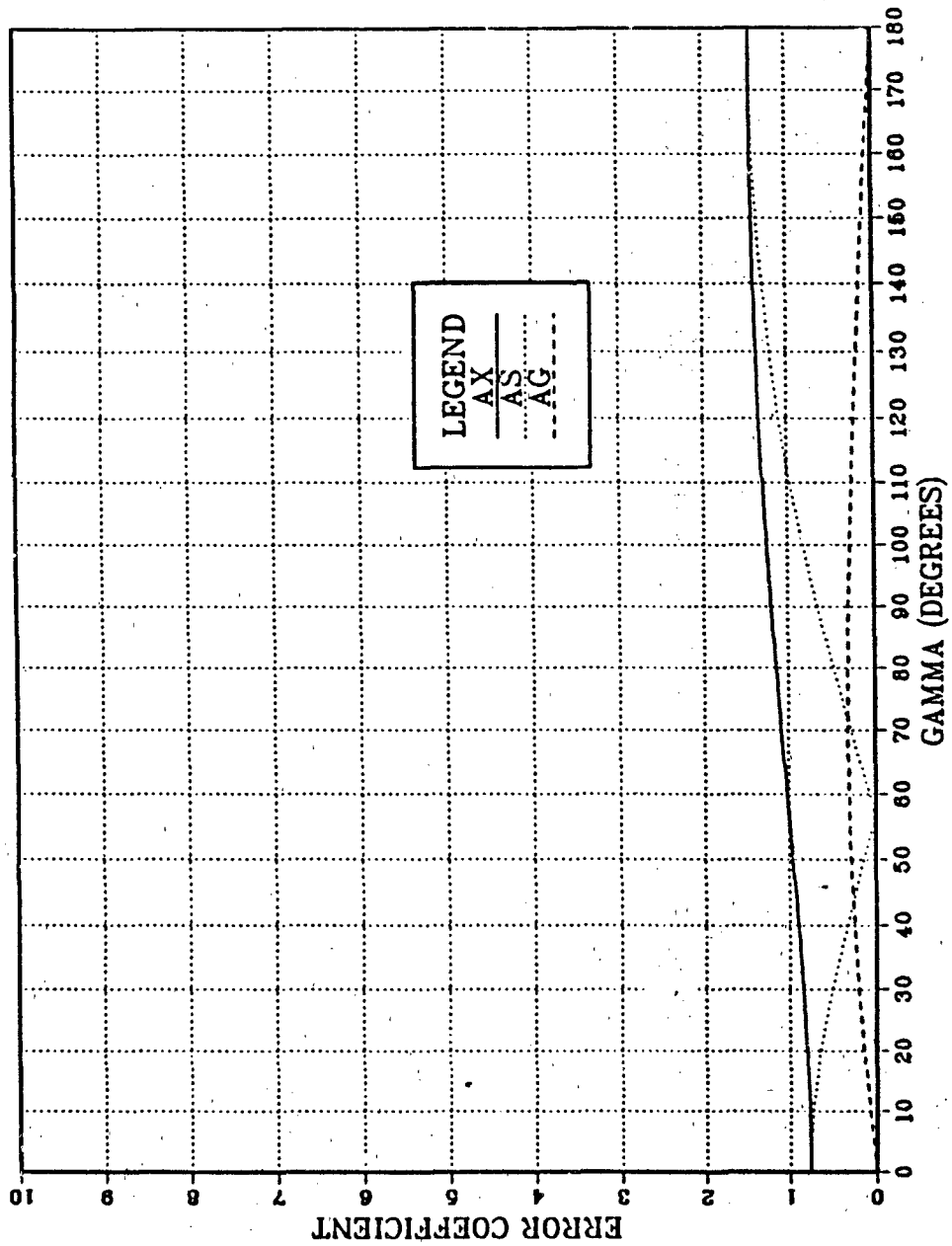

Figure 7 Error vs. Angle for e=0.3

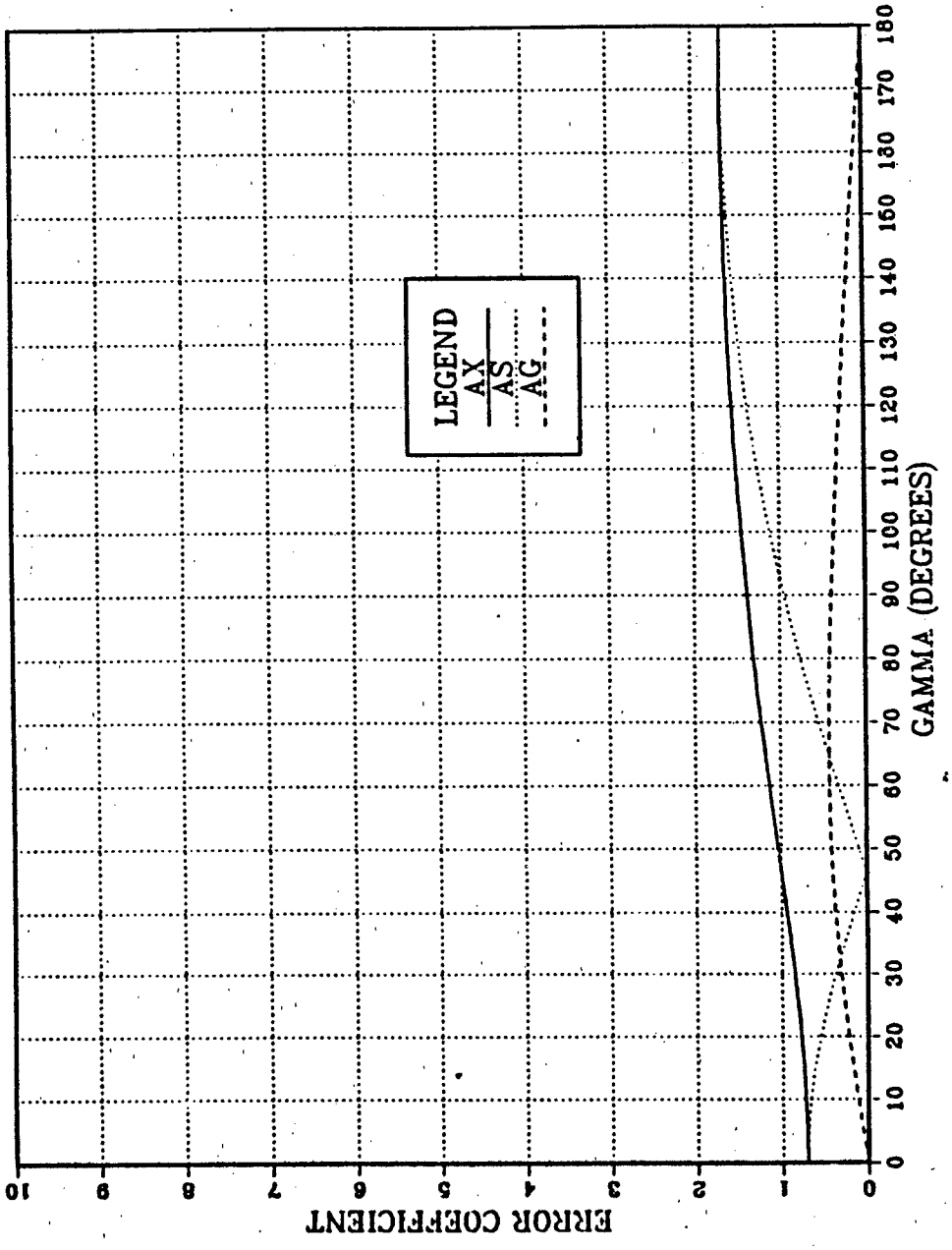

Figure 8 Error vs. Angle for e=0.4

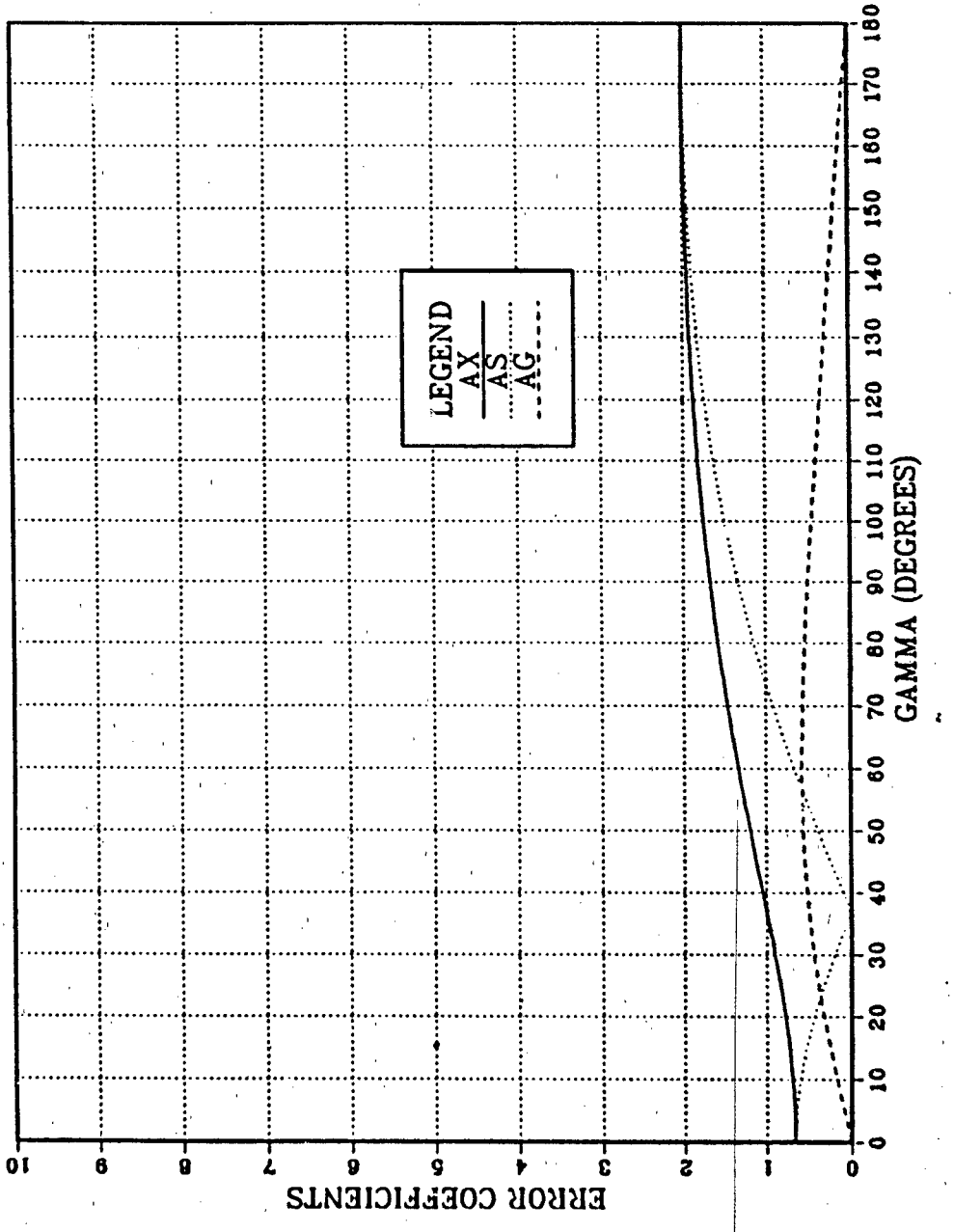

Figure 9 Error vs. Angle for e=0.5

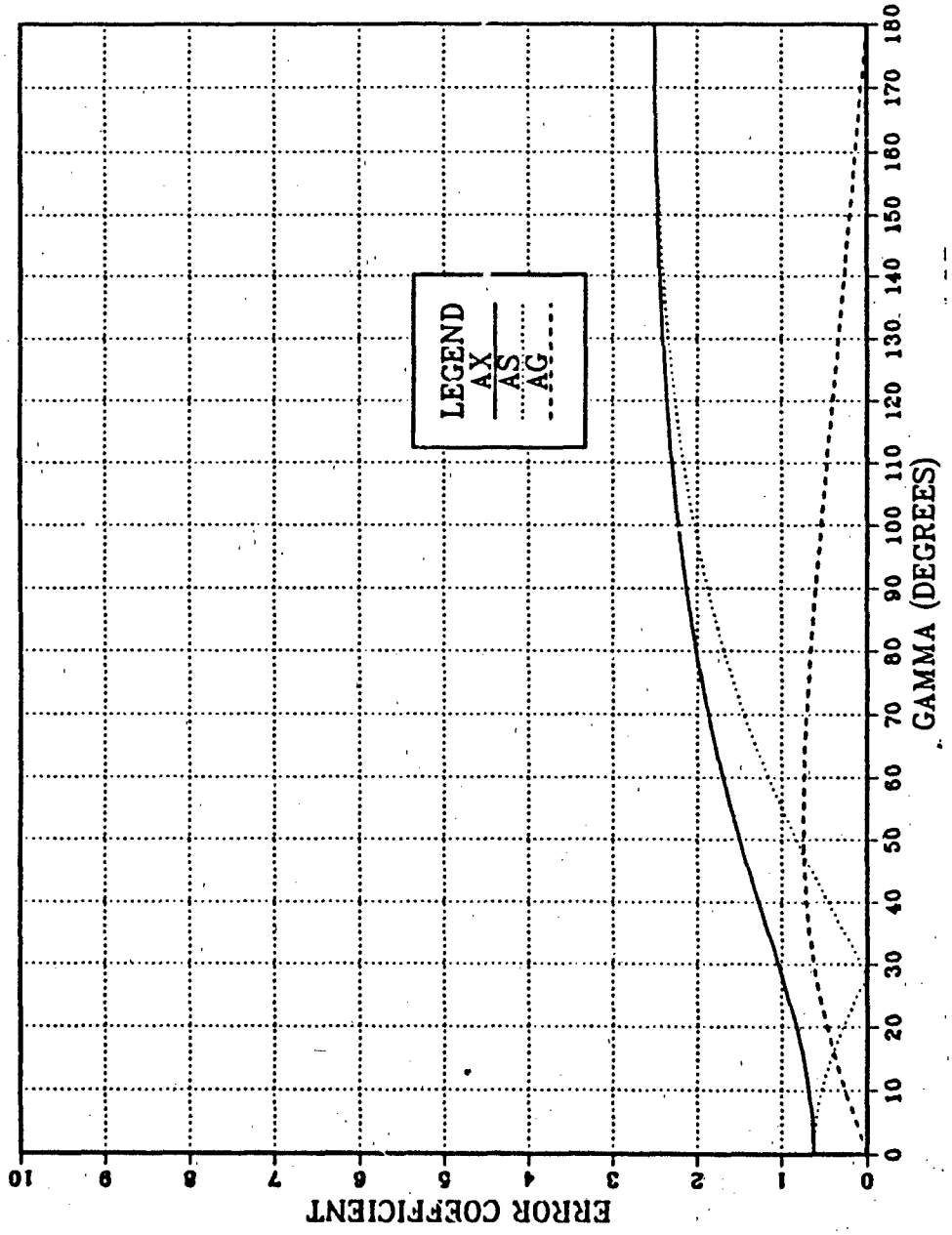

Figure 10 Error vs. Angle for e=0.6

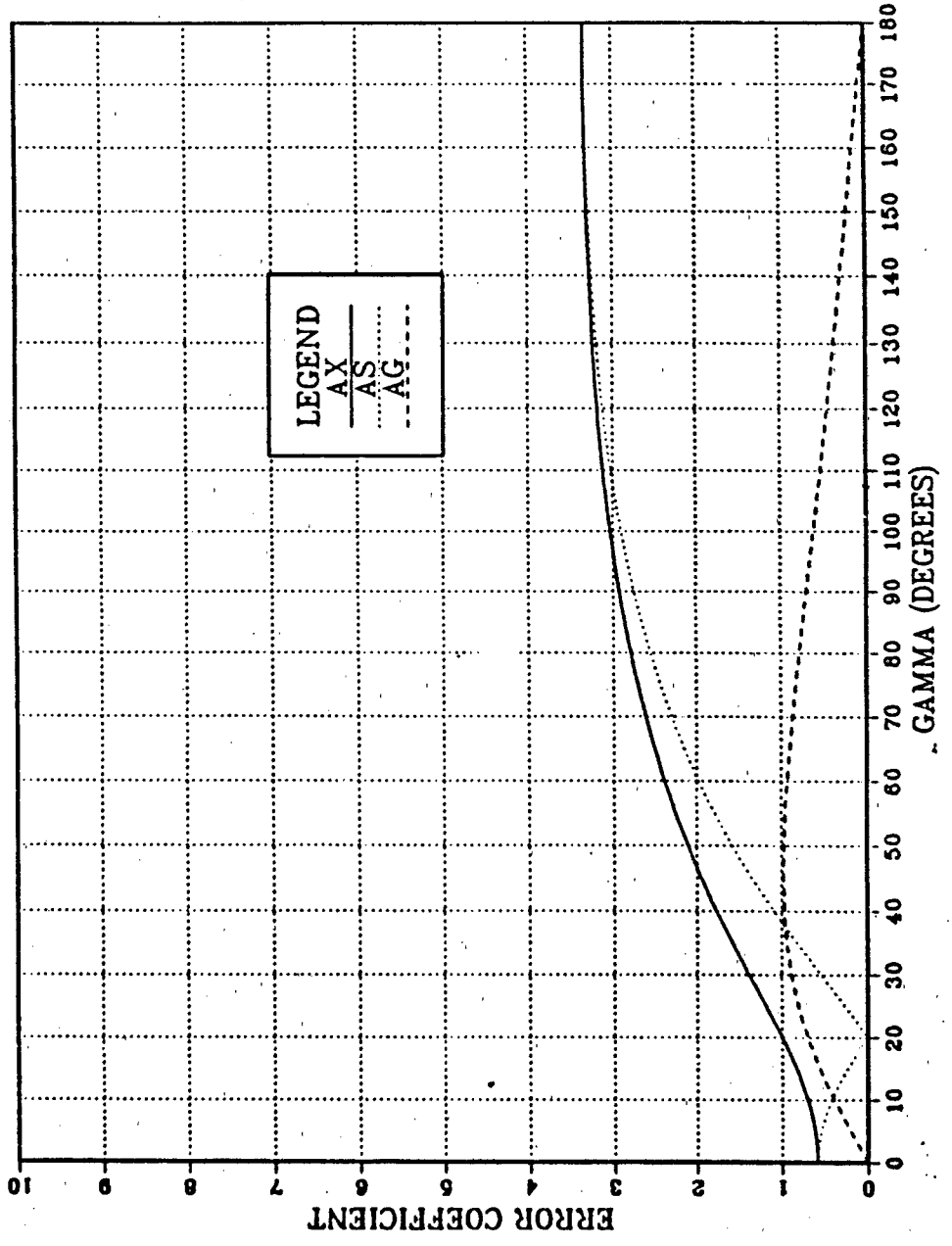

Figure 11 Error vs. Angle for e=0.7

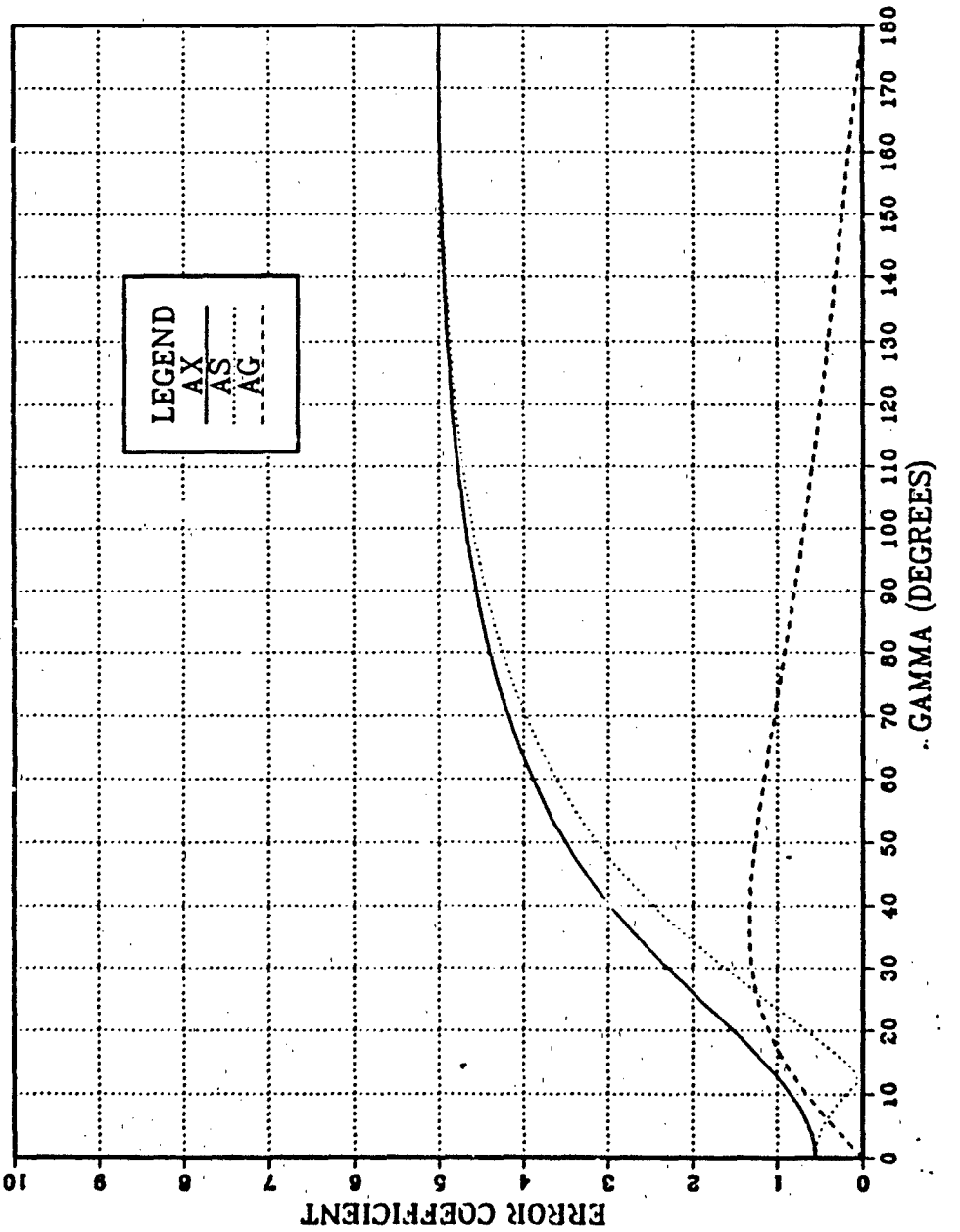

Figure 12 Error vs. Angle for e=0.8

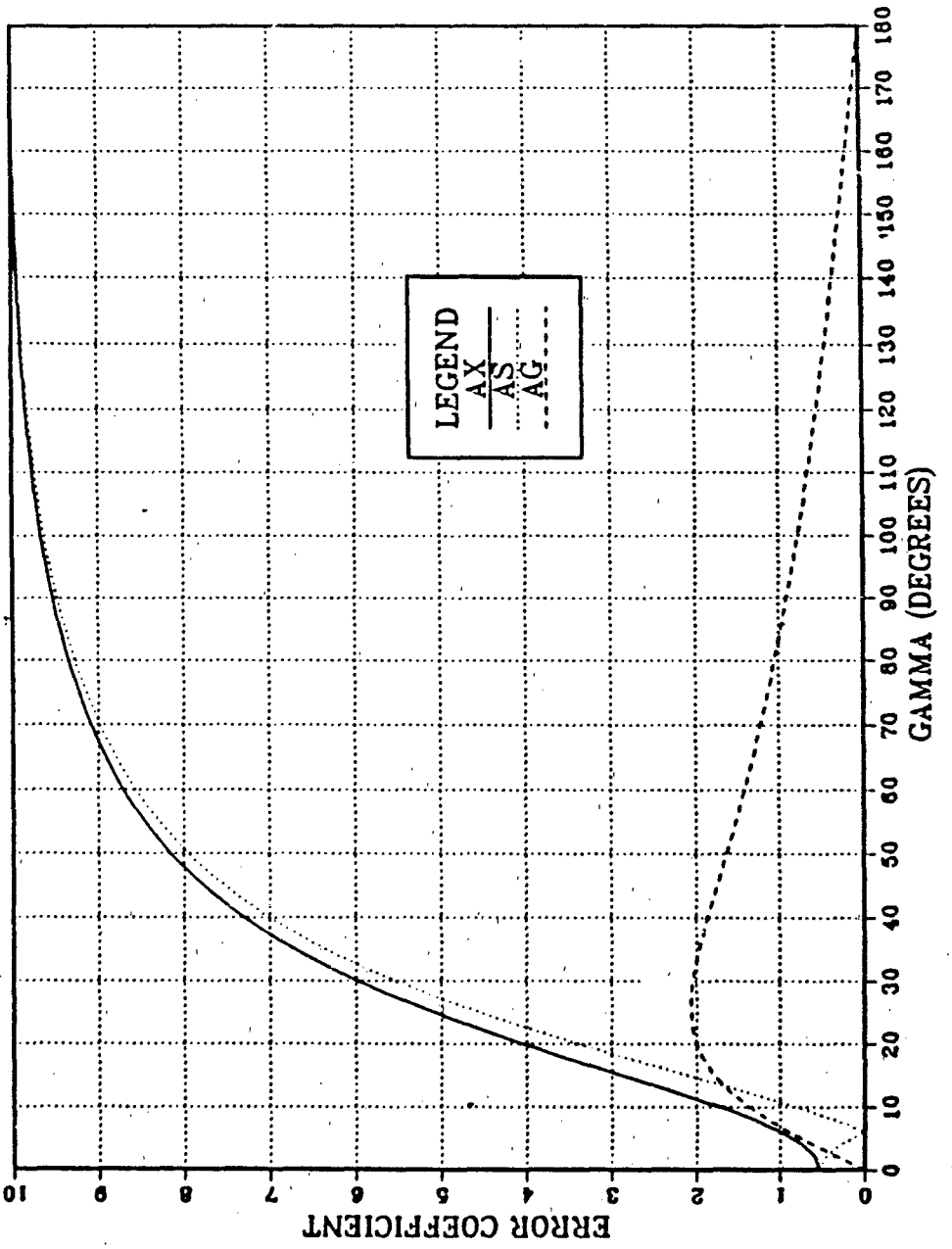

Figure 13 Error vs. Angle for e=0.9

B. VERIFICATION OF MODEL

Verification of this model was done by graphical confirmation (elliptical) of theoretical expressions. The three variables that contribute errors to a particular bistatic geometry are t_x, t_s, and γ. The variables t_x and t_s determines the eccentricity of the ellipse and γ determines the location of the target on that ellipse. For each of the three curves, one of the three variables is assumed to be in error by approximately 10% while the remaining two variables were considered to be exactly determined. This forces the two remaining terms to become zero, and the fractional error, $\Delta R/R$, is now equal to the one remaining term. The fractional error can be crudely determined from the elliptical figure at various values of γ and compared with the value of the appropriate coefficient A_x, A_s, or A_c obtained from one of the figures (Figures 5 - 13) for a corresponding value of e. The first of the terms to be validated is the A_x term. Two ellipses are drawn in Figure 14 that share the same focal points, because t_s is held constant, thus guaranteeing a constant inter-focal distance S. Ellipse 1 has an eccentricity of 0.80. If the t_x value is increased by 10%, the eccentricity can be seen from

$$e = \frac{t_s}{t_x}, \quad for\ U=V \tag{4.1}$$

to be reduced to 0.73. Ellipse 2 is the ellipse that results from this reduced eccentricity with the same source to receiver spacing. At any given value of γ, there are two corresponding values of R, and the difference between these two is ΔR. This value is divided by the mean of the two R's, to give $\Delta R/R$. In Figure 14 there are four comparisons made at separate values of γ. There is an illustration of what the

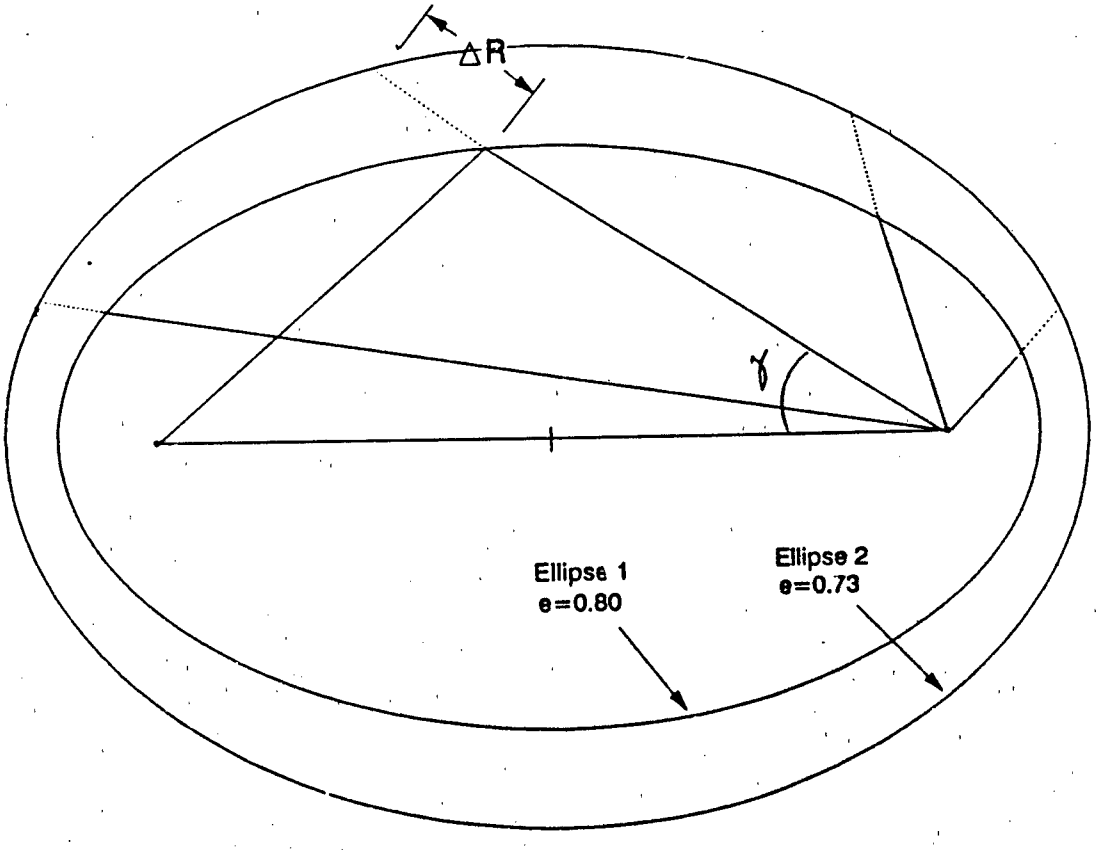

Figure 14 Validation of A_χ

a small value of γ, the $\Delta R/R$ should be relatively small since R has its largest values here. As γ increases, ΔR increases as R decreases resulting in a rapid climb of $\Delta R/R$ which is confirmed in Figures 11 and 12. Finally, as γ approaches 180°, ΔR and R remain constant which explains the asymptotic behavior of the function at higher values of γ.

The next term, A_s, is validated through Figure 15, where t_x and γ are held constant and t_s is decreased by 10%. Ellipse 1 in Figure 15 is the original geometry for a given t_s and

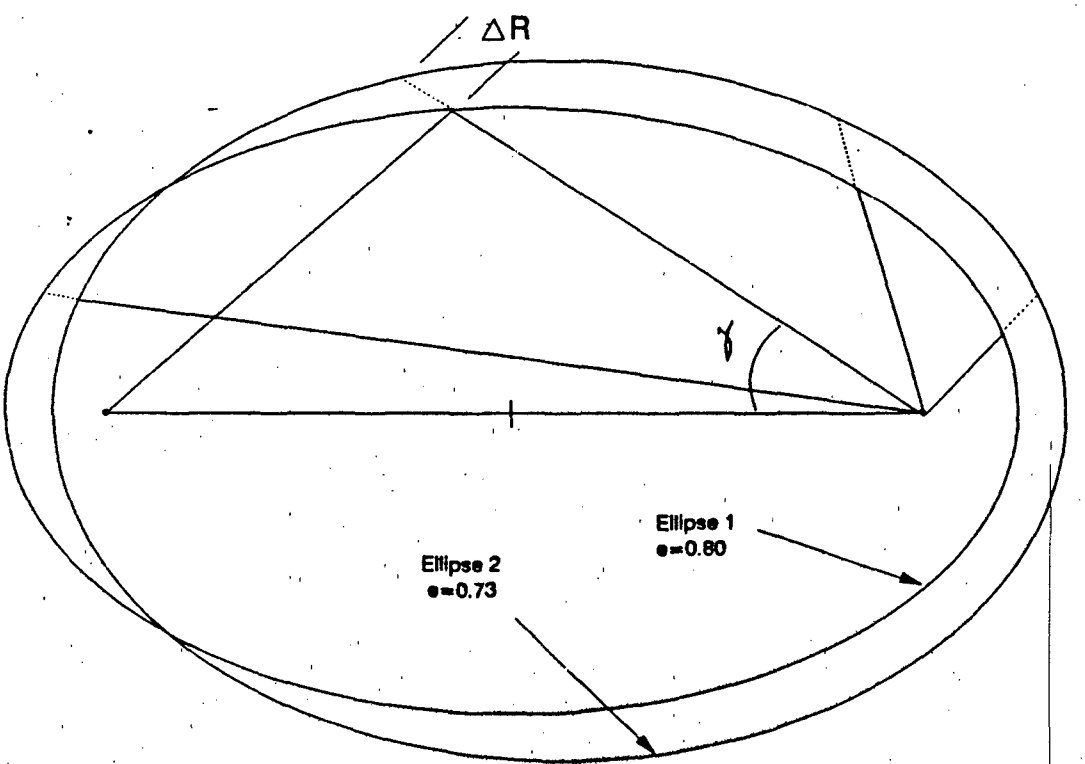

Figure 15 Validation of A_s

ellipse 2 shows the geometry with t_s reduced by 10%, which gives a reduced eccentricity. This graphic is most interesting because there is an immediate explanation for the

zero value of A_s at about 20° in Figure 11. Shortly beyond this value of γ, the plot behaves quite similarly to the A_x plot. As γ increases beyond about 90°, the graph again demonstrates asymptotic behavior.

The validation of the A_G function is shown in figure 16.

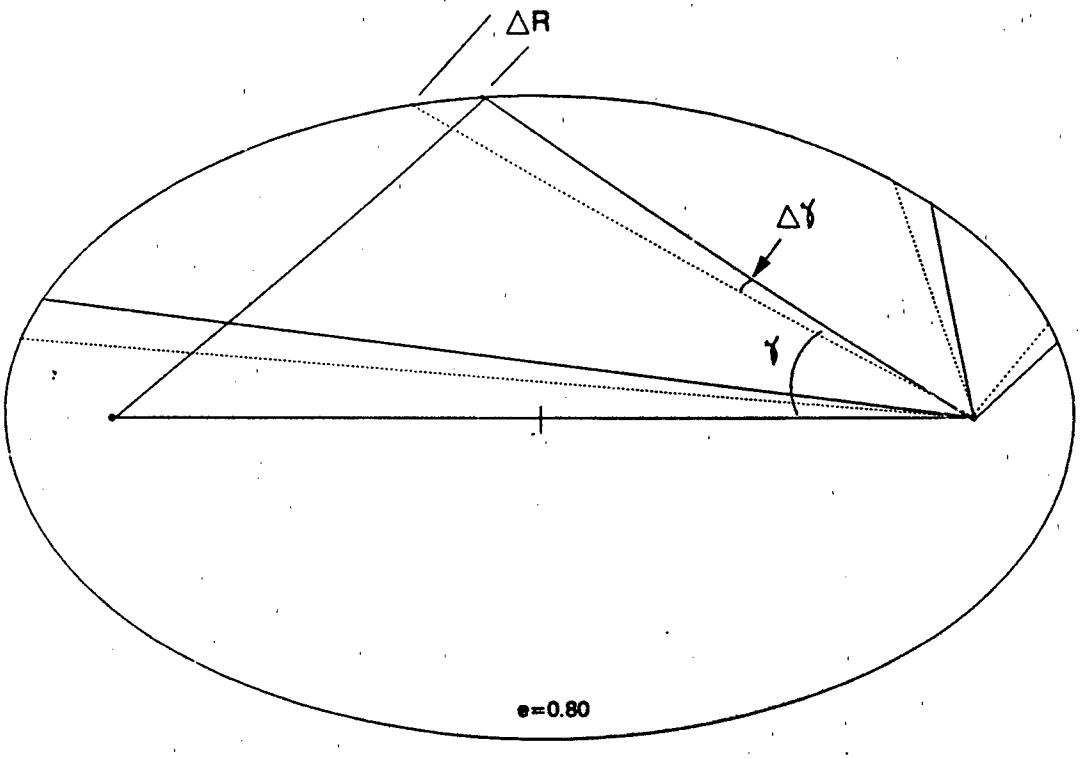

Figure 16 Validation of A_G

The validation in this case requires that t_x and t_s remain constant while γ is permitted to change slightly. Since t_x and t_s remain constant, so must e remain the same. Thus there is only one ellipse to be considered here. Figure 16 shows four angles γ and four associated $\Delta\gamma$'s shown by the dotted

lines. The difference in length between the dotted line and the solid line is the ΔR value. Note that ΔR is zero where γ is either 0° or 180°. The graphic demonstrates that for higher values of e, as in this case, there will be a maximum value of ΔR between 20° and 50°, followed by a gradual decline to zero as γ increases to 180°. For lower values of eccentricity, the ΔR value reaches its maximum close to 90° and has a much smaller value than in the case of larger eccentricity.

The geometrical analysis resulting in Figures 14 through 16 gives a graphical interpretation of the errors arrived at algebraically in Chapter III. From these figures one can readily see which errors are more significant for the various conditions that may occur in the range problem.

V. EXAMPLE CASES

It is helpful to illustrate use of the analysis by applying it to practical problems. The following examples will demonstrate the previously mentioned error propagation in cases that might be encountered at sea. These examples will be approached as if the calculation were conducted from input provided by Sonar Control onboard an ASW ship. The uncertainty numbers used in these examples are not necessarily realistic, but are useful in the demonstration of the method. The first three examples are of geometries of low eccentricity while the remaining examples are of high eccentricity.

A. EXAMPLE 1: LOW ECCENTRICITY; NO UNCERTAINTIES IN V

For the first example assume that the mean sound speed is the same over both paths, that is, U equals V. Figure 17 is a diagram of an elliptical arrangement of low eccentricity; S is less than X. Suppose that the following data are provided:

$$\gamma = 110^\circ \pm 1^\circ$$
$$t_s = 42.62 \pm 0.01\ s$$
$$t_x = 213.9 \pm 0.03\ s$$
$$V = 4990\ ft/s$$
$$U = V$$
$$conversion = 6076\ ft/nm$$

Calculated values of the various terms in the equations are then as follows:

$$e = \frac{t_s}{t_x} = 0.2$$

$$R = \frac{V(t_x^2 - t_s^2)}{2\,(t_x - t_s \cos\gamma)} = 78.966\ nm$$

$$\frac{\Delta V}{V} = 0$$

$$\frac{\Delta t_x}{t_x} = 0.000140$$

$$\frac{\Delta t_s}{t_s} = 0.000235$$

$$\Delta\gamma = 0.0174\ rad$$

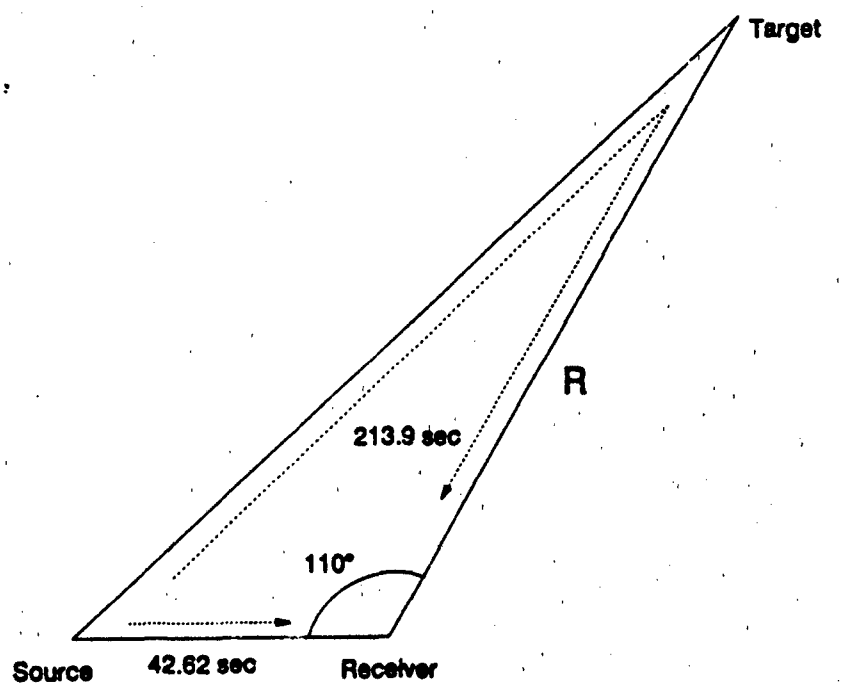

Figure 17 Example Case, Low Eccentricity

$$A_X = \left(\frac{2}{1-e^2} - \frac{1}{1-e\cos\gamma}\right) = 1.147$$

$$A_S = \left(\frac{-2e}{1-e^2} + \frac{\cos\gamma}{1-e\cos\gamma}\right) = -0.737$$

$$A_G = \frac{-e\sin\gamma}{1-e\cos\gamma} = -0.176$$

If it is assumed that the uncertainties are random (independent) then the RMS fractional error may be calculated from (3.11) in which it is assumed that U = V, so that $\tau_X = t_X$, and also that $\Delta V/V$ equals 0:

$$\frac{1}{R}(\Delta R)_{rms} = \sqrt{A_X^2\left(\frac{\Delta t_X}{t_X}\right)^2 + A_S^2\left(\frac{\Delta t_S}{t_X}\right)^2 + A_G^2(\Delta\gamma)^2} = 0.003075$$

Thus the expected uncertainty in range, ΔR, should be about ± 500 yards or less.

B. EXAMPLE 2: LOW ECCENTRICITY; UNCERTAINTY IN V

Assume the same situation as in Example 1, but now assume an uncertainty in V of ± 3 ft/s. Now, we have an $\Delta V/V$ value of 0.0006 in addition to the other errors in Example 1. The term $\Delta V/V$ in (3.11) is now not zero, but $\tau_X = t_X$ as before. The fractional error is now

$$\frac{1}{R}(\Delta R)_{rms} = \sqrt{\left(\frac{\Delta V}{V}\right)^2 + A_X^2\left(\frac{\Delta t_X}{t_X}\right)^2 + A_S^2\left(\frac{\Delta t_S}{t_X}\right)^2 + A_G^2(\Delta\gamma)^2} = 0.003133$$

Note that the error in $\Delta V/V$ in this case does not have a large effect.

C. EXAMPLE 3: LOW ECCENTRICITY; U AND V UNEQUAL

In this example the situation is the same as in Example 1 but now let U = 5040 ft/s so that U is not equal to V. The data to be used are in this case:

$$\gamma = 110^\circ \pm 1^\circ$$
$$t_s = 42.62 \pm 0.01\, s$$
$$t_x = 213.9 \pm 0.03\, s$$
$$V = 4990\, ft/s$$
$$U = 5040\, ft/s$$

Now, it is necessary to rescale t_x as discussed in Chapter II,C.,(2.22):

$$\tau_x = \frac{U}{V} t_x = 1.010\, t_x$$

From this point, analysis proceeds as in Example 1.

$$e = \frac{t_s}{\tau_x} = 0.198$$

$$R = \frac{V(\tau_x^2 - t_s^2)}{2(\tau_x - t_s \cos\gamma)} = 79.873\, nm$$

$$A_x = \left(\frac{2}{1-e^2} - \frac{1}{1-e\cos\gamma}\right) = 1.145$$

$$A_S = \left(\frac{-2e}{1-e^2} + \frac{\cos\gamma}{1-e\cos\gamma}\right) = -0.733$$

$$A_G = \frac{-e\sin\gamma}{1-e\cos\gamma} = -0.174$$

Now, we use (3.11) with $\tau_X = t_X$, and $\Delta V/V = 0$, to get

$$\frac{1}{R}(\Delta R)_{rms} = \sqrt{A_X^2\left(\frac{\Delta\tau_X}{\tau_X}\right)^2 + A_S^2\left(\frac{\Delta t_S}{\tau_X}\right)^2 + A_G^2(\Delta\gamma)^2} = 0.003133$$

The mean square fractional error is now somewhat greater than that in Example 1, as might be expected.

D. EXAMPLE 4: HIGH ECCENTRICITY; NO UNCERTAINTIES IN V

Assume that the mean sound speed is the same over both paths. Figure 18 is a diagram of an elliptical arrangement of high eccentricity, which means that the source and receiver are generally farther apart than the target and receiver. Suppose that the following data are provided:

$$\gamma = 110^\circ \pm 1^\circ$$
$$t_S = 85.23 \pm 0.01\ s$$
$$t_X = 106.54 \pm 0.03\ s$$
$$V = 4990\ ft/s$$
$$U = V$$

$$e = \frac{t_S}{t_X} = 0.8$$

$$R = \frac{V(t_x^2 - t_s^2)}{2\,(t_x - t_s \cos\gamma)} = 12.37\ nm$$

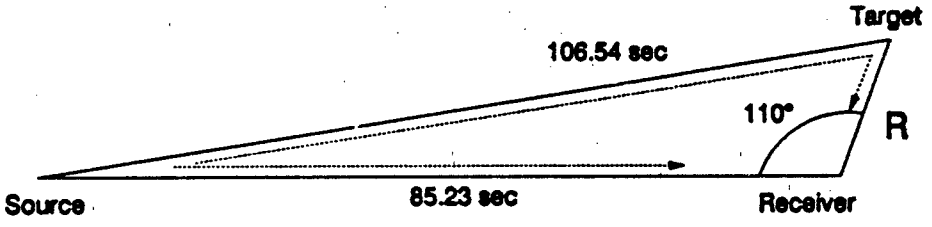

Figure 18 Example Case, High Eccentricity

$$A_X = \left(\frac{2}{1-e^2} - \frac{1}{1-e\cos\gamma}\right) = 4.770$$

$$A_S = \left(\frac{-2e}{1-e^2} + \frac{\cos\gamma}{1-e\cos\gamma}\right) = -4.713$$

$$A_G = \frac{-e\sin\gamma}{1-e\cos\gamma} = -0.590$$

Equation (3.11) gives for this case:

$$\frac{1}{R}(\Delta R)_{rms} = \sqrt{\left(\frac{\Delta V}{V}\right)^2 + A_X^2\left(\frac{\Delta \tau_X}{\tau_X}\right)^2 + A_S^2\left(\frac{\Delta t_S}{\tau_X}\right)^2 + A_G^2(\Delta\gamma)^2} = 0.010398$$

Note that ΔR/R is almost a factor of 3 greater than in the previous examples of low eccentricity. However, for the geometry, the actual range error is 260 yards, about half of the expected error of the earlier cases. It is important to point out that the fractional error ΔR/R is a fairly sensitive fuction of eccentricity, but the actual range error depends on the size of the ellipse.

E. EXAMPLE 5: UNCERTAINTY IN V

Here the same data are provided as in Example 4, but in this case V has uncertainty of ± 3 ft/s. This time we have $\Delta V/V = 0.0006$ to be included in the RMS calulation, as was used in Example 2, and again $\tau_X = t_X$. The RMS fractional uncertainty is thus

$$\frac{1}{R}(\Delta R)_{rms} = \sqrt{\left(\frac{\Delta V}{V}\right)^2 + A_X^2\left(\frac{\Delta \tau_X}{\tau_X}\right)^2 + A_S^2\left(\frac{\Delta t_S}{\tau_X}\right)^2 + A_G^2(\Delta\gamma)^2} = 0.010398 .$$

The expected range error in this case is also about 260 yards.

F. EXAMPLE 6: U AND V UNEQUAL

In this example, as in Example 3, assume that the same data are provided as in the two previous examples except that U is not equal to V and there is no uncertainty in V. Thus,

$$\gamma = 110° \pm 1°$$
$$t_S = 85.23 \pm 0.01\ s$$
$$t_X = 106.54 \pm 0.03\ s$$
$$V = 4990\ ft/s$$
$$U = 5040\ ft/s$$

Again we must rescale t_X by using τ_X:

$$\tau_X = \frac{U}{V} t_X = 1.01 t_X$$

and the process proceeds as in Example 4.

$$e = \frac{t_S}{\tau_X} = 0.792$$

Use (3.11) with $t_X \rightarrow \tau_X$, and $\Delta V/V = 0$ to get a fractional error

$$R = \frac{V(\tau_x^2 - t_s^2)}{2\,(\tau_x - t_s \cos\gamma)} = 12.959\ nm$$

$$A_X = \left(\frac{2}{1-e^2} \cdot\cdot \frac{1}{1-e\cos\gamma}\right) = 4.580$$

$$A_S = \left(\frac{-2\,e}{1-e^2} + \frac{\cos\gamma}{1-e\cos\gamma}\right) = -4.520$$

$$A_G = \frac{-e\,\sin\gamma}{1-e\cos\gamma} = -0.586$$

$$\frac{1}{R}(\Delta R)_{rms} = \sqrt{A_X^2\left(\frac{\Delta\tau_x}{\tau_x}\right)^2 + A_S^2\left(\frac{\Delta t_s}{\tau_x}\right)^2 + A_G^2(\Delta\gamma)^2} = 0.010327$$

The expected range error is here about 270 yards, slightly larger than in Examples 4 and 5.

VI. CONCLUSION

A. DISCUSSION AND RESULTS

Improved quieting techniques by submarines have been very effective in reducing the exploitable emissions for passive sensors. On the other hand, detection by active sonar is independent of the submarine's quieting efforts and gives the added bonus of providing an immediate determination of range to the target. Thus, active sonar seems to give certain obvious advantages. Additionally, a bistatic sonar technique increases detection range of active sonar and reduces the vulnerability of the active platform.

This thesis has examined a method of predicting range and range uncertainties in bistatic sonar operations. The method described here offers flexibility over conventional methods that rely heavily on communication between source and receiver for successful operations. Operational methods that use the separation distance S are often preferred over those that require a knowledge of the mean sound speed V, especially near fronts and eddies where the mean sound speed may change drastically in a few miles. However, this thesis has shown that the preference of using the baseline over the mean sound speed is unfounded.

As shown in the previous chapter, the range error is controlled to a great extent by the eccentricity of the range ellipse, the largest errors occurring in the cases of high

eccentricity. Examples are given to provide representative applications of the range Equation (2.3) and to give the estimates of the range errors.

We have seen that fractional error $\Delta R/R$ tends to be small when $\bullet$ is small, although dependance on γ is still quite significant. This suggests that small base-line geometries (small values of S leading to small $\bullet$) are to be preferred if these are operationally feasible.

LIST OF REFERENCES

1. Kinsler, L.E., Frey, A.R., Coppens, A.B. and Sanders, J. V., Fundamentals of Acoustics, 3rd Ed., p. 411, Wiley, 1982.

2. Urick, R.J., Principles of Underwater Sound, 3rd Ed., p. 7, McGraw-Hill, 1983.

3. Stefanick, Tom, Strategic Antisubmarine Warfare and Naval Strategy, pp. 217-219, Lexington Books, 1987.

4. BBN Systems and Technologies Corporation Technical Memorandum No. W1068, Fundamentals of Bistatic Active Sonar, by Henry Cox, pp. 4-5, Jul 88.

5. Free, Lou, "Disposition of Source and Receiver in Bistatic Sonar," inter-office memorandum, Naval Underwater Systems Center (NUSC), 9 Feb 87.

6. Analysis and Technology, Inc., Geometric Sensitivity of Bistatic Target Range Estimater to Main Blast Localization Errors, by D.C. Ghen, p. 1-1, 8 Mar 90.

7. Angolia, J.R., LTCOL, USA, and et al,, The U.S. War Machine, pp. 50-52, Salamander Books Ltd., 1978.

8. Summary Technical Report of the National Defense Research Committee, A Survey of Subsurface Warfare in World War II, by J. B. Conant, Chairman, p. 15, 1946.

9. Office of Deputy chief of Naval Operations (ASW Division), "Antisubmarine Warfare; Meeting the Challenge," pp. 24-25, Apr 90.

INITIAL DISTRIBUTION LIST

		No. Copies
1.	Defense Technical Information Center Cameron Station Alexandria, Virginia 22304-6145	2
2.	Library, Code 52 Naval Postgraduate School Monterey, California 93943-5000	2
3.	Chairman, Code PH Physics Department Naval Postgraduate School Monterey, California 93943-5000	1
4.	Prof. Alan B. Coppens, Code PH/Cz Naval Postgraduate School Monterey, California 93943-5000	2
5.	Prof. Harvey A. Dahl, Code PH/Dh Naval Postgraduate School Monterey, California 93943-5000	1
6.	Mr. Peter Herstein Naval Underwater Systems Center (Code 33A) New London Laboratory New London, Connecticut 06320-5594	2
7.	Mr. Carl Nawrocki Naval Underwater Systems Center (Code 33B) New London Laboratory New London, Connecticut 06320-5594	1
8.	Mr. Lou Free Naval Underwater Systems Center (Code 01B) New London Laboratory New London, Connecticut 06320-5594	1
9.	Mr. Jim Kyle Naval Underwater Systems Center (Code 01Y) New London Laboratory New London, Connecticut 06320-5594	1
10.	Mr. Joe Geary Naval Underwater Systems Center (Code 212) New London Laboratory New London, Connecticut 06320-5594	1

11. Commander Surface Warfare Development Group 1
Naval Amphibious Base, BLDG 1602, (Code N30)
Little Creek, Virginia 23521-5160

12. LT J.C. Nygaard 1
Department Head Class 118
Surface Warfare Officer School Command
Newport, Rhode Island 02841-5012